Thermal stability of ultrathin amorphous carbon overcoats for heat-assisted magnetic recording

J. Xie and K. Komvopoulos

Department of Mechanical Engineering, University of California, Berkeley, CA 94720, USA

Abstract

Ultrathin hydrogenated amorphous carbon (a-C:H) films deposited by plasma-enhanced chemical vapor deposition (PECVD) and hydrogen-free amorphous carbon (a-C) films of similar thickness deposited by filtered cathodic vacuum arc (FCVA) were subjected to rapid thermal annealing (RTA) and their structural stability was investigated by cross-sectional transmission electron microscopy (TEM) and electron energy loss spectroscopy (EELS). While RTA at 650°C for 1 s increased the thickness of the intermixing layer and decreased the sp^3 content of the a-C:H films, the a-C films demonstrated indiscernible changes in both thickness and sp^3 content. The TEM and EELS results of this study reveal the superior structural stability FCVA a-C films compared with PECVD a-C:H films, suggesting that FCVA a-C films are prime candidates for protective overcoats in applications where rapid heating is of concern, such as heat-assisted magnetic recording.

I. INTRODUCTION

Although ultrathin amorphous carbon (*a*-C) films are used as protective overcoats in numerous applications, mainly because of their high hardness and excellent wear and corrosion resistance,[1–3] very little is known about their structural stability under rapid heating conditions. The demands for ultrahigh storage densities[4–6] have motivated the evolution of new information storage technologies that are not restricted by the superparamagnetic limit, such as heat-assisted magnetic recording,[7,8] which uses a laser-optical system integrated into the magnetic head to locally heat a fine-grained magnetic medium of high magnetic anisotropy energy density above its Curie temperature in order to instantaneously decrease its coercivity and enable information to be stored in the form of single bits by the transducer of the magnetic head. However, the rapid and repetitive temperature excursions encountered with this technology may degrade the structure of the ultrathin *a*-C film by destabilizing atomic carbon bonding.[9,10]

The structure of *a*-C films can be characterized by the dominance of trigonal (sp^2) and tetrahedral (sp^3) carbon atom bonding, which strongly depends on the deposition process. Plasma-enhanced chemical vapor deposition (PECVD)[11,12] and filtered cathodic vacuum arc (FCVA)[13–15] are considered to be the most effective deposition methods for synthesizing continuous ultrathin (≤5 nm thick) *a*-C films with good mechanical properties. However, because the surface and intermixing layers of FCVA *a*-C films exhibit a lower sp^3 content than the bulk layer,[16–21] the overall structure, composition, and nanomechanical properties of ultrathin FCVA *a*-C films might be inferior compared with those of relatively thick *a*-C films because their structure is dominated by those of the surface and intermixing layers which possess low sp^3 contents. As a result, variations in the cross-sectional uniformity of ultrathin *a*-C films may negatively impact their mechanical behavior.[22–25]

In previous studies focused on the structural stability of ultrathin *a*-C films, X-ray photoelectron spectroscopy (XPS), X-ray reflectivity (XRR), and visible resonant Raman spectroscopy were used to discern structural differences between as-deposited and thermally treated (annealed) *a*-C films. For example, a Raman spectroscopy study[26] of the structural stability of 1.5-nm-thick diamondlike carbon (dlc)

films revealed insignificant changes in the structure of FCVA dlc films, but significant carbon loss for sputtered dlc films. In another study,[27] an increase in sp^2 hybridization and a decrease in thickness of 5-nm-thick PECVD carbon films were observed after rapid laser heating. Multi-wavelength Raman, XRR, and XPS investigations[28] have shown that rapid heating to 659 ˚C for 1 s of hydrogenated dlc films synthesized by PECVD, sputtering, and FCVA causes a decrease in sp^3 fraction but not detectable changes in film density and hydrogen content. Despite important insight into the effect of rapid heating on the quality of ultrathin carbon films obtained from these studies, the used characterization methods are subjected to film thickness and signal intensity limitations. In particular, XPS cannot provide detailed information about the structure of each layer existing in ultrathin FCVA a-C films, XRR fails to accurately measure the density of ultrathin films possessing a multilayered structure,[29,30] and Raman analysis uses an extrapolation method to indirectly estimate the sp^3 fraction. To detect changes in the cross-sectional film structure, it is necessary to directly measure the sp^3 content with nanometer resolution. Cross-sectional electron energy loss spectroscopy (EELS) is a suitable method for studying the through-thickness structure of ultrathin films because it provides high spatial and energy resolution.

A review of the literature, including the studies mentioned above, indicates that information about structural changes (e.g., sp^3 content) of the interface (intermixing), bulk, and surface layers of a-C films subjected to rapid heating is sparse. Therefore, knowledge of the structural stability of ultrathin a-C films subjected to rapid thermal annealing (RTA), as revealed by cross-sectional structural and compositional changes, is of particular importance. The objective of this study is to elucidate and compare the structural stability of ultrathin a-C films deposited by two competing methods, i.e., PECVD and FCVA. Changes in carbon concentration, atomic carbon hybridization, and thickness of a-C films subjected to RTA were studied by high-resolution transmission electron microscopy (HRTEM) and cross-sectional EELS. HRTEM and EELS results are contrasted to quantify differences in the structural stability of PECVD and FCVA ultrathin a-C films.

II. EXPERIMENTAL METHODS

A. Film Deposition

Substrates (1×1 cm^2) cut from the 2.5-in.-diameter glass disks coated with a ~100-nm-thick NiTa alloy were coated with ~5-nm-thick a-C films deposited by PECVD using acetylene (C_2H_2) as the film precursor or by FCVA. The density (determined from XRR measurements) and hydrogen content of the PECVD a-C films were found equal to ~2.0–2.1 g/cm^3 and 30–40%, respectively. To deposit a-C films on similar substrates by FCVA, glass/NiTa substrates coated with a PECVD a-C film were loaded onto the substrate holder of a custom-made FCVA system[31,32] and the PECVD overcoat was sputtered off by bombarding with 500-eV Ar$^+$ ions generated by a 64-mm Kaufman ion source (Commonwealth Scientific, Alexandria, VA) under a working pressure of ~2×10^{-4} Torr and a 60° Ar$^+$ ion incidence angle measured from the normal to the substrate surface. XPS analysis confirmed that, under these conditions, the PECVD a-C film was fully removed after 6 min of Ar$^+$ ion sputtering (Fig. 1). After cooling the substrate for 5 min and reaching a base pressure of $<5 \times 10^{-7}$ Torr, the substrate stage was rotated to a position normal to the C$^+$ ion flux and plasma arcing at the cathode (99.99% pure graphite) surface was induced by a mechanical striker. The plasma was stabilized by a cusp-configuration magnetic field which was applied to the cathode,[31] while the potential and the current between the graphite cathode and the anode were kept at ~24 V and ~89 A, respectively. The magnetic field generated by out-of-plane S-shape electromagnetic coils was used to filter out any macroparticles and/or droplets ejected from the cathode, ensuring the arrival of only high-purity (~99.99%) C$^+$ ions at the filter exit. The current of the auxiliary, upstream, and downstream coils was set at 30.5, 30.9, 29.6 A, respectively. To control the C$^+$ ion energy during film deposition, an optimum pulsed bias voltage of -100 V magnitude and 25 kHz frequency was applied to the substrate used in all the FCVA film depositions. For uniformity in sputter etching and film deposition in the radical direction, during Ar$^+$ ion bombardment and FCVA deposition the substrate was rotated at 60 rpm. To deposit ultrathin FCVA films of thickness similar to that of the PECVD films, the deposition time was fixed at 12 s.

B. Rapid Thermal Annealing

RTA experiments were performed in a heating chamber integrated with a computer control system (RTP-600xp, Modular Process Technology). The specimen was heated by tungsten-halogen lamps and the temperature rise was measured with a thermocouple placed in contact with the backside of the specimen holder. The heating rate during RTA was equal to 105 ± 8.5 °C/s. During RTA, the equipment was purged with a gas mixture of 8000 sccm N_2 and 2000 sccm O_2. The maximum temperature and time during RTA were equal to 650 °C and 1 s, respectively. Further details on the RTA equipment are given elsewhere.[33]

C. TEM and EELS

Cross-sectional HRTEM specimens were prepared by mechanical grinding, dimpling, and surface finishing by ion milling. To differentiate the epoxy glue from the a-C film and to distinguish the EELS carbon signal of the a-C film from the epoxy glue, a Au capping layer of 5–10 nm thickness was sputtered onto the specimen surface before specimen bonding. More details about the TEM specimen preparation method used in this study can be found elsewhere.[34,35]

HRTEM images and EELS spectra were acquired with a microscope (F20 UT, FEI Tecnai) operated at 200 kV, equipped with a CCD camera (2048 × 2048 pixels) placed 42 mm behind a Gatan imaging filter. The EELS collection semi-angle was set at 16.3 mrad. A 150-μm C2 aperture and a 9.4-mrad C2 semi-angle were used in this study. The spatial resolution of the scanning TEM (STEM) without a monochromator is 0.14 nm. From the full-width at half-maximum of the zero-loss peak, the energy resolution was found to be less than 0.58 eV. Considering that the bandgap difference between sp^2 and sp^3 is ~0.8–0.9 eV, an energy resolution of less than 0.58 eV is sufficient for distinguishing sp^2 from sp^3 hybridizations.

III. RESULTS AND DISCUSSION

Figure 2 shows cross-sectional HRTEM images of PECVD and FCVA a-C films obtained before and after RTA. (The different layers in each image are labeled in Fig. 2(b)). All images show four distinct regions: (1) NiTa alloy layer, (2) a-C film, (3) Au capping layer, and (4) epoxy glue. A comparison of the HRTEM images shown in Fig. 2 does not show any apparent changes in film thickness or sp^2 clustering due to RTA in either type of film. Thus, it may be interpreted that film oxidation and dissociation did not occur under the present RTA conditions. However, Table I shows a notable change in the average thickness of the PECVD films. While the average thickness of the FCVA a-C films was not affected by RTA, the mean thickness of the PECVD a-C films increased from 4.61 to 5.45 nm.

The cross-sectional elemental composition of the a-C films was investigated by analytical EELS. For carbon atoms, the range of the characteristic K-edge spectra for determining the sp^2 and sp^3 fractions of a-C films is from 280 to 305 eV. The pre-edge peak at 285 eV is due to the excitation of electrons from the ground-state 1s core level to the vacant π^*-like anti-bonding states, whereas the edge from 290 eV is due to the excitation of electrons from the 1s core level to the σ^* states.[36] Therefore, information about the elemental composition can be extracted from the ionization edges. The π^* peak is fitted with a Gaussian distribution, while the σ^* peak is integrated in the energy range from 290 to 305 eV, to minimize plural scattering effects. The area ratio of these two peaks is proportional to the relative number of π^* and σ^* orbitals, which is 1/3 for 100% sp^2 and 0/4 for 100% sp^3.

The fraction x of sp^2 bonded carbon atoms in the a-C films is given by[36]

$$\frac{(\pi^*/\sigma^*)_{\text{film}}}{(\pi^*/\sigma^*)_{\text{std}}} = \frac{3x}{4-x} \tag{1}$$

where the standard (std) specimen is assumed to consist of 100% sp^2 evaporated carbon. More details about the curve fitting method and calculation of the sp^3 fraction are given elsewhere.[16]

Figure 3 shows the effect of RTA on the structure of the PECVD and FCVA a-C films. The normalized intensity was obtained by integrating the EELS spectrum in the range of 280–305 eV, whereas

6

the depth profiles of the sp^3 fraction were calculated from the C K-edge spectra using Eq. (1). It can be seen that RTA decreased the sp^3 fraction of the PECVD a-C films and the carbon intensity shifted to the inner layer, presumable due to hydrogen depletion, as shown by Raman spectroscopy.[33] The sp^3 fraction and carbon concentration reveal the existence of the five distinct regions: (1) *substrate* (the carbon signal intensity is almost zero because it originates from the NiTa alloy); (2) *intermixing layer* (both the carbon concentration and sp^3 content increase rapidly); (3) *bulk film* (the carbon concentration stabilizes at ~100%, whereas the sp^3 fraction remains fairly constant); (4) *surface layer* (both the carbon concentration and the sp^3 fraction decrease sharply); (5) *capping layer* (the low intensity of the carbon signal is attributed to carbon from the ambient adsorbed onto the surface of the Au capping layer).

Table I gives the thickness of the intermixing, bulk, and surface layers and the average sp^3 fraction of the bulk layer of the a-C films before and after RTA. The sum of the thicknesses of all the layers comprising the a-C films is referred to as the total thickness. The agreement between TEM and EELS results of the total film thickness is fairly good. The thickness of the surface and bulk layers of PECVD a-C films are similar before and after RTA, while the intermixing layer thickness increased from 2.3 nm to 3.2 nm, presumably a result of carbon diffusion. The bulk layer of the FCVA a-C films exhibits a higher sp^3 fraction relatively to the PECVD a-C films. Moreover, RTA caused the sp^3 fraction of the bulk layer of PECVD films to decrease by 4.5%, indicating the occurrence of carbon graphitization and/or $sp^3 \rightarrow sp^2$ rehybridization. In contrast, RTA did not affect the thickness, carbon intensity, or sp^3 content of the FCVA a-C films.

IV. CONCLUSIONS

The effect of RTA on the structure, composition, and thickness of PECVD and FCVA a-C films was examined by HRTEM and EELS. It was shown that RTA at 650 °C for 1 s increases the thickness of the intermixing layer by ~0.9 nm and reduces the sp^3 fraction of the bulk layer of PECVD films by 4.5%.

Under the same RTA conditions, the FCVA *a*-C films exhibited insignificant changes in both thickness and sp^3 content, revealing a superior structural stability over PECVD films.

REFERENCES

[1] A. Grill, Diam. Relat. Mater. **8**, 428 (1999).

[2] J. Robertson, Mater. Sci. Eng. R: Reports **37**, 129 (2002).

[3] C. Casiraghi, J. Robertson, and A. C. Ferrari, Mater. Today **10**, 44 (2007).

[4] R. Wood, J. Magn. Magn. Mater. **321**, 555 (2009).

[5] Z. Z. Bandić and R. H. Victora, Proc. IEEE **96**, 1749 (2008).

[6] Z.-M. Yuan, B. Liu, T. Zhou, C. K. Goh, C. L. Ong, C.M . Cheong, and L. Wang, IEEE Trans. Magn. **45**, 5038 (2009).

[7] M.H . Kryder, E. C. Gage, T. W. McDaniel, W. A. Challener, R. E. Rottmayer, G. Ju, Y.-T. Hsia, and M. F. Erden, Proc. IEEE **96**, 1810 (2008).

[8] B. C. Stipe et al., Nature Photonics **4**, 484 (2010).

[9] D. S. Grierson, A. V. Sumant, A. R. Konicek, T. A. Friedmann, J. P. Sullivan, and R. W. Carpick, J. Appl. Phys. **107**, 033523 (2010).

[10] R. Kalish, Y. Lifshitz, K. Nugent, and S. Prawer, Appl. Phys. Lett. **74**, 2936 (1999).

[11] J. Robertson, Thin Solid Films **383**, 81 (2001).

[12] K. L. Choy, Prog. Mater. Sci. **48**, 57 (2003).

[13] B. Petereit, P.Siemroth, H. H. Schneider, and H. Hilgers, Surf. Coat. Technol. **174**, 648 (2003).

[14] A. Anders, *Cathodic Arcs: From Fractal Spots to Energetic Condensation*, Springer Series on Atomic, Optical, and Plasma Physics, Springer Science and Business Media, New York, NY, 2008.

[15] S. Xu, B. K. Tay, H. S. Tan, L. Zhong, Y. Q. Tu, S. R. P. Silva, and W. I. Milne. J. Appl. Phys. **79**, 7234 (1996).

[16] N. Wang and K. Komvopoulos, J. Mater. Res. **28**, 2124 (2013).

[17]M. P. Siegal, P. N. Provencio, D. R. Tallant, R. L. Simpson, B. Kleinsorge, and W. I. Milne, Appl. Phys. Lett. **76**, 2047 (2000).

[18]C. A. Davis, G. A. J. Amaratunga, and K. M. Knowles, Phys. Rev. Lett. **80**, 3280 (1998).

[19]C. A. Davis, K. M. Knowles, and G. A. J. Amaratunga, Surf. Coat. Technol. **76–77**, 316 (1995).

[20]E. Riedo, F. Comin, J. Chevrier, F. Schmithusen, S. Decossas, and M.Sancrotti, Surf. Coat. Technol. **125**, 124 (2000).

[21]Y. Lifshitz, S. R. Kasi, J. W. Rabalais, and W. Eckstein, Phys. Rev. B **41**, 10468 (1990).

[22]A. C. Ferrari, Surf. Coat. Technol. **180–181**, 190 (2004).

[23]C. Casiraghi, A. C. Ferrari, J. Robertson, R. Ohr, M. V. Gradowski, D. Schneider, and H. Hilgers, Diam. Relat. Mater. **13**, 1480 (2004).

[24]C. Casiraghi, A. C. Ferrari, R. Ohr, D. Chu, and J. Robertson, Diam. Relat. Mater. **13**, 1416 (2004).

[25]M. G. Beghi, A. C. Ferrari, K. B. K. Teo, J. Robertson, C. E. Bottani, A. Libassi, and B. K. Tanner, Appl. Phys. Lett. **81**, 3804 (2002).

[26]S. Kundu, N. Dwivedi, N. Satyanarayana, R. J. Yeo, J. Ahner, P. M. Jones, and C. S. Bhatia, ACS Appl. Mater. Interf. **7**, 158 (2014).

[27]P. M. Jones, J. Ahner, C. L. Platt, H. Tang, and J. Hohlfeld, IEEE Trans. Magn. **50**, 144 (2014).

[28]F. Rose, N. Wang, R. Smith, Q.-F. Xiao, H. Inaba, T. Matsumura, Y. Saito, H. Matsumoto, Q. Dai, B. Marchon, F. Mangolini, and R. W. Carpick, J. Appl. Phys. **116**, 123516 (2014).

[29]A. C. Ferrari, A. Libassi, B. K. Tanner, V. Stolojan, J. Yuan, L. M. Brown, S. E. Rodil, B. Kleinsorge, and J. Robertson, Phys. Rev. B **62**, 11089 (2000).

[30]C. M. Mate, B. K. Yen, D. C. Miller, M. F. Toney, M. Scarpulla, and J. E. Frommer, IEEE Trans. Magn. **36**, 110 (2000).

[31]H.-S. Zhang and K. Komvopoulos, Rev. Sci. Instrum. **79**, 073905 (2008).

[32]H.-S. Zhang and K. Komvopoulos, J. Appl. Phys. **105**, 083305 (2009).

[33]N. Wang, K. Komvopoulos, F. Rose, and B. Marchon, J. Appl. Phys. **113**, 083517(2013).

[34]D. Wan and K. Komvopoulos, J. Mater. Res. **19**, 2131 (2004).

[35]N. Wang and K. Komvopoulos, IEEE Trans. Magn. **48**, 2220 (2012).

[36]J. J. Cuomo, J. P. Doyle, J. Bruley, and J. C. Liu, Appl. Phys. Lett. **58**, 466 (1991).

Table I. Comparison of total thickness, layer thickness, and sp^3 content of bulk layer of a-C films deposited by PECVD and FCVA obtained before and after rapid thermal annealing at 650 °C for 1 s.

Deposition method	Rapid thermal annealing	Thickness (nm)					sp^3 (%) bulk layer
		total (TEM)	total (EELS)	intermixing layer	bulk layer	surface layer	
PECVD	before	4.56 ± 0.24	5.6	2.3	1.8	1.5	37.63 ± 0.44
	after	5.47 ± 0.50	6.5	3.2	1.8	1.5	33.10 ± 1.24
FCVA	before	4.61 ± 0.13	5.9	1.9	2.3	1.7	59.14 ± 1.36
	after	4.63 ± 0.26	6.1	2.1	2.3	1.7	58.07 ± 1.44

List of Figures

Fig. 1   XPS spectrum of obtained after 6 min of 500-eV Ar^+ ion bombardment. The spectrum confirms the complete removal of the PECVD a-C film from the NiTa/glass substrate.

Fig. 2   Cross-sectional HRTEM images of a-C films deposited by (a–c) PECVD and (d–f) FCVA. Overview images of a-C films deposited on NiTa/glass substrates (a, d) and close-up views of a-C films obtained (b, e) before and (c, f) after RTA. Contrast and structural differences reveal four distinct regions: (1) NiTa alloy layer, (2) a-C film, (3) Au capping layer, and (4) epoxy glue.

Fig. 3   Cross-sectional depth profiles of normalized intensity of C-K edge and sp^3 fraction calculated from the C K-edge spectra of a-C films deposited by (a) PECVD and (b) FCVA showing differences before and after RTA. The dashed lines indicate the boundaries between adjacent regions.
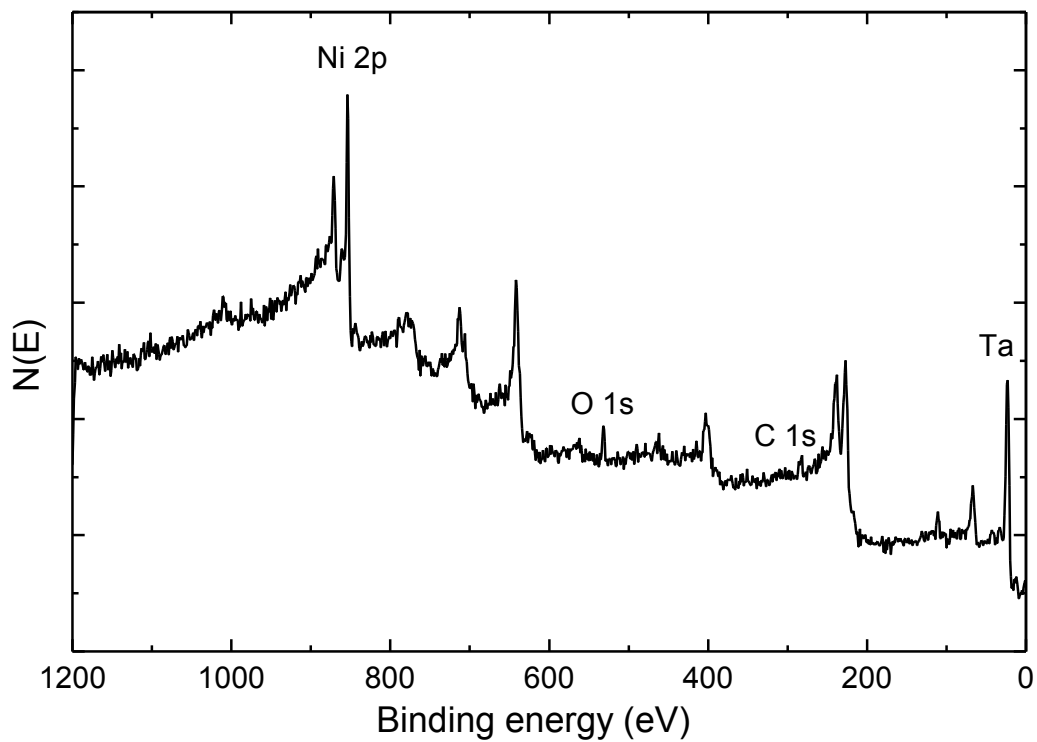
Fig. 1.   XPS spectrum of obtained after 6 min of 500-eV Ar$^+$ ion bombardment. The spectrum confirms

the complete removal of the PECVD a-C film from the NiTa/glass substrate.
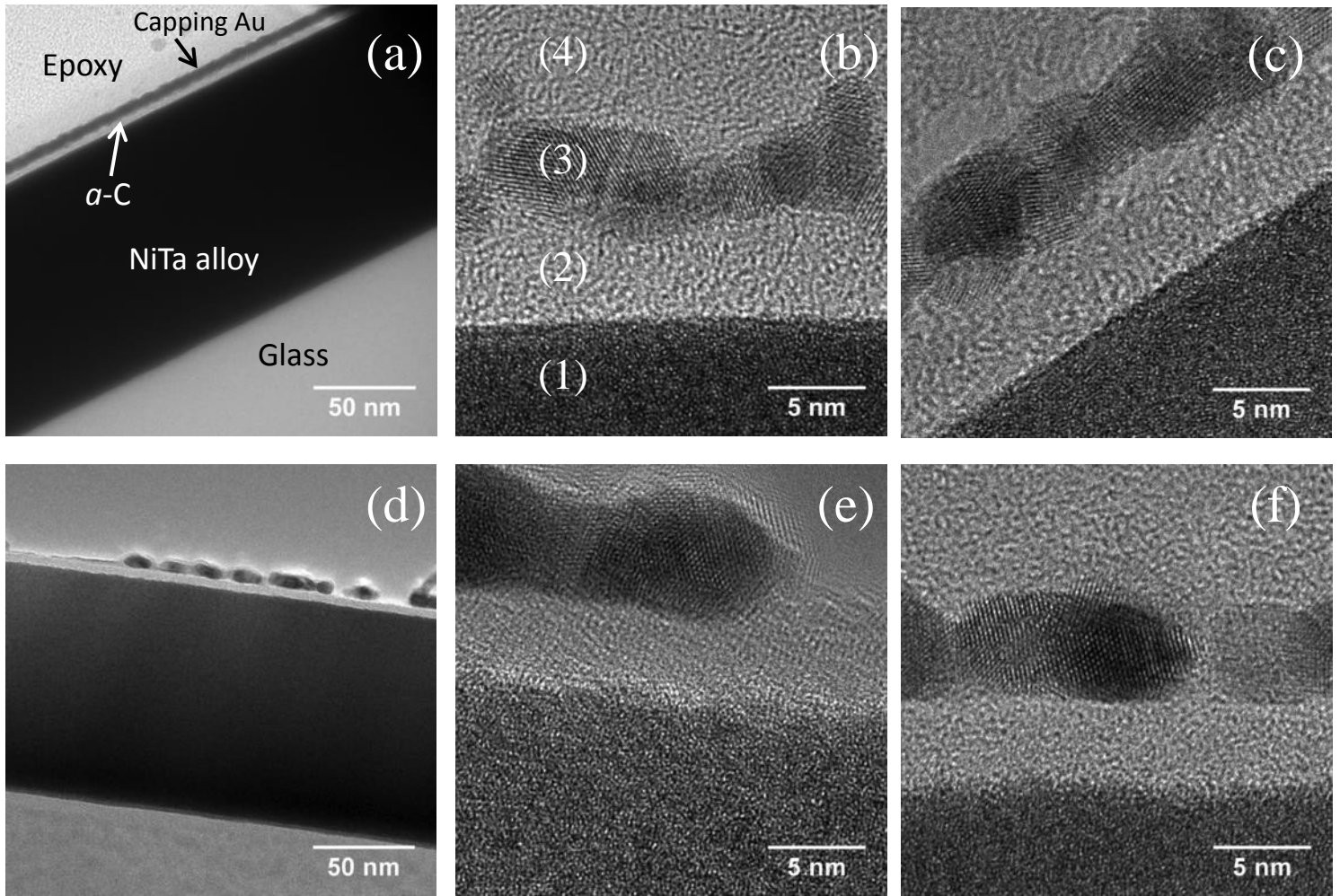
Fig. 2. Cross-sectional HRTEM images of *a*-C films deposited by (a–c) PECVD and (d–f) FCVA. Overview images of *a*-C films deposited on NiTa/glass substrates (a, d) and close-up views of *a*-C films obtained (b, e) before and (c, f) after RTA. Contrast and structural differences reveal four distinct regions: (1) NiTa alloy layer, (2) *a*-C film, (3) Au capping layer, and (4) epoxy glue.
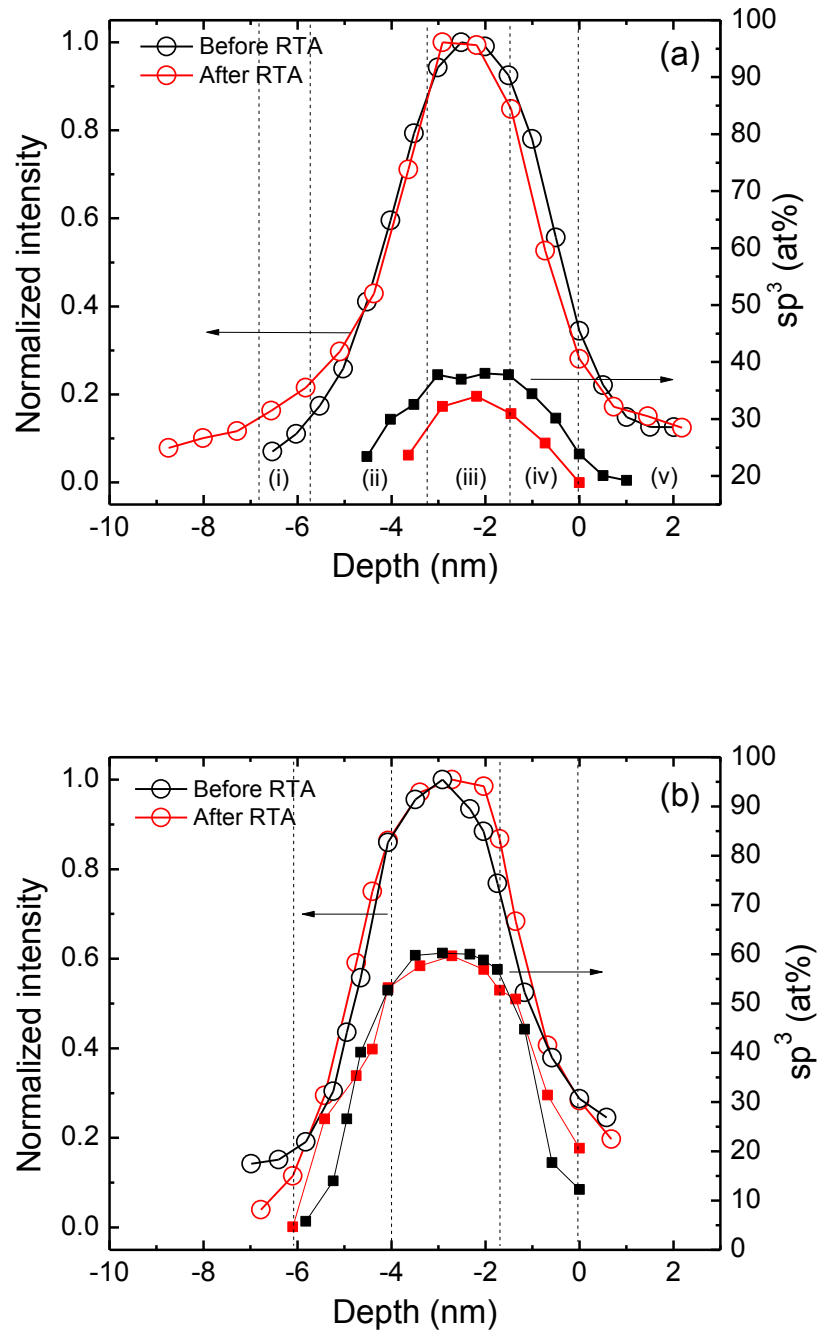
Fig. 3. Cross-sectional depth profiles of normalized intensity of C-K edge and sp^3 fraction calculated from the C K-edge spectra of *a*-C films deposited by (a) PECVD and (b) FCVA showing differences before and after RTA. The dashed lines indicate the boundaries between adjacent regions.